

CHALMERS



UNIVERSITY OF GOTHENBURG

*PREPRINT 2013:6*

# Uncertainties in Damage Prediction of Wind Turbine Blade under Random Gust

S. VENKATESH  
SUNETRA SARKAR  
IGOR RYCHLIK

*Department of Mathematical Sciences*

*Division of Mathematical Statistics*

CHALMERS UNIVERSITY OF TECHNOLOGY

UNIVERSITY OF GOTHENBURG

Gothenburg Sweden 2013



Preprint 2013:6

# **Uncertainties in Damage Prediction of Wind Turbine Blade under Random Gust**

S. Venkatesh, Sunetra Sarkar and Igor Rychlik

Department of Mathematical Sciences  
Division of Mathematical Statistics  
Chalmers University of Technology and University of Gothenburg  
SE-412 96 Gothenburg, Sweden  
Gothenburg, April 2013

Preprint 2013:6  
ISSN 1652-9715

---

Matematiska vetenskaper  
Göteborg 2013

# Uncertainties in Damage Prediction of Wind Turbine Blade under Random Gust

S.Venkatesh

Department of Aerospace Engineering  
Indian Institute of Technology Madras  
Chennai 600036 India  
Email: svenky.87@gmail.com

Sunetra Sarkar (Corresponding Author)  
Department of Aerospace Engineering  
Indian Institute of Technology Madras  
Chennai 600036 India

Tel: +91 44 2257 4024, Fax: +91 44 2257 4002  
Email: sunetra.sarkar@gmail.com

Igor Rychlik

Department of Mathematical Sciences  
Chalmers University of Technology  
SE-41296, Gothenburg, Sweden  
Email: igor.rychlik@gmail.com

April 18, 2013

## Abstract

In the design of wind turbine structures, aeroelastic stability is of utmost importance. The bending-torsion oscillation problem of a representative rotor blade section with structural nonlinearity has been considered. The system is subjected to horizontal random gust modeled as a stationary process. Uncertainty quantification in highlighting the relative importance of different sources of uncertainty on aeroelastic system stability, consequently its fatigue and failure is a crucial step of aeroelastic design. Effect of different sources of uncertainty on the fatigue damage estimate of the blade are studied in the present aeroelastic problem. The effect of the following on the fatigue damage estimate of the blade is reported in this work, structural parameter, choice of aeroelastic model (modeling error) and also the stress selection criteria for the damage estimate. The structural parameter randomness is modeled through polynomial chaos expansion in analyzing its effect on the damage estimate. The unsteady inviscid flow-field in the aeroelastic model is resolved analytically and also using a higher fidelity vortex lattice algorithm and the relative effect on damage is seen. Finally, the effect of fatigue damage criteria selection is also observed. The damage calculation is done for torsion only, bending only and also for multiaxial stress situations. Multiaxial stresses are converted to an ‘equivalent’ one by using a signed von Mises criterion. A linear damage accumulation rule has been used to estimate the risk for fatigue damage.

## keywords

bending-torsion flutter, uncertainty quantification, polynomial chaos expansion, fatigue damage.

## Nomenclature

$m$  = Structural mass per unit span  
 $h$  = Plunge displacement in meters  
 $I_\alpha$  = Mass moment of inertia about elastic axis  
 $S_\alpha$  = First moment of inertia  
 $c_\alpha, c_h$  = Viscous damping coefficients in pitch and plunge  
 $K_\alpha, K_h$  = Linear stiffness coefficients in pitch and plunge  
 $K_{\alpha_1}, K_{h_1}$  = Non linear stiffness coefficients in pitch and plunge  
 $L_\alpha, M_\alpha$  = Unsteady aerodynamic lift and moment  
 $L_u$  = Horizontal length scale of the gust  
 $a_h$  = Non-dimensional distance from airfoil mid-chord to elastic axis  
 $b$  = Airfoil semi-chord  
 $C_L$  = Lift coefficient  
 $C_M$  = Pitching moment coefficient  
 $r_\alpha$  = Radius of gyration about elastic axis  
 $u(t)$  = Longitudinal turbulence  
 $U$  = Non-dimensional speed  
 $x_\alpha$  = Non-dimensional distance from elastic axis to center of mass  
 $\alpha$  = Pitch angle of airfoil  
 $\varepsilon$  = Non-dimensional plunge displacement  
 $\beta_\alpha, \beta_\varepsilon$  = Cubic spring coefficients in pitch and plunge  
 $\zeta_\alpha, \zeta_\varepsilon$  = Viscous damping ratio in pitch and plunge  
 $\mu$  = Airfoil/air mass ratio  
 $\tau$  = Non-dimensional time  
 $\omega_\alpha, \omega_\varepsilon$  = Uncoupled natural frequency in pitch and plunge respectively  
 $\bar{\omega}$  = Natural frequency ratio in plunge and pitch  
 $\phi$  = used in many contexts as standard notations and is defined locally as appropriate.

## Introduction

Flutter oscillation can occur in flexible structural systems when it is subjected to high wind forces. It is self induced in nature and becomes a recipe for disaster when not properly controlled, as the resulting oscillation amplitude could be quite high. Such structures should be designed with carefully selected parameters in order to avoid flutter from taking place. In the presence of parametric uncertainties, the flutter margin can become sensitive to such parameters once again. An uncertainty quantification to estimate the propagation of uncertainty is crucial to evaluate the probability of failure or fatigue damage. The paper gives methodology for studying different sources for uncertainties in fatigue life prediction of wind turbine blade subjected to gusts. The following typical uncertainties will be considered; modeling error uncertainty in predicting the aerodynamic loads acting on a blade; choice of fatigue criterion and uncertainty in system parameters used to model the blade's motions.

The modeling error uncertainty will be studied by comparing fatigue life predictions for two different aeroelastic models of body wake interaction used to evaluate aerodynamic loads acting on the blade. The methods will be presented in sections entitled 'Analytical Model for  $C_L$  and  $C_M$  in (3)' (in more detail in Appendix 1) and ' $C_L$  and  $C_M$  Estimated by Means of Unsteady Vortex Lattice Method'. The first one is the classical formulation given by Wagner<sup>1</sup> in which the airfoil body is approximated as a flat plate and the unsteady wake behind the trailing edge is assumed to be fixed behind the body. The second model uses an unsteady vortex lattice method (UVLM). This model considers the actual shape of the airfoil and the wake is discretized into computational elements forming a freely rolling wake structure. The airfoil body is the section of a model blade treated as a cantilever beam fixed at the hub with arbitrarily chosen blade parameters. The aeroelastic system is subject to a horizontal random gust which is a stationary normal process having von Karman spectrum. The presence of gust makes the airfoil oscillate randomly and the classical bifurcation theory cannot be applied<sup>2</sup>. Uncertainties due to choice of fatigue criterion will be discussed in section entitled 'Uncertainty in Fatigue Damage Prediction'. The criteria to predict damage rates will be discussed in section entitled 'Fatigue Damage Criteria'. Common engineering approach combining linear damage accumulation hypothesis with constant amplitude experiments (S-N data) will be employed. The differences in fatigue life predictions will be investigated while consid-

ering stresses due to torsion, bending separately and also by combining the stresses into a signed von Mises stress. S-N curves established from the torsion and tensile loads on a representative material will be used.

As mentioned before, proper design of blade is crucial for reliable and safe use of an aeroelastic system. In particular, flutter oscillations in blades are very undesired motions. In section entitled ‘Governing Equations of Motion’ coupled non-linear oscillators are used to describe the motion (plunge and pitch) of the blade. An important parameter  $\bar{\omega}$ , which is the natural frequency ratio in plunge and pitch, is assumed not perfectly known and hence modeled as a random variable. In the realm of uncertainty quantification, influence of random parameters on response of interest have traditionally been analyzed with the help of Monte Carlo Simulation (MCS). Of late however a spectral uncertainty quantification tool called polynomial chaos expansion (PCE), pioneered by Ghanem and Spanos<sup>3</sup>, has been put into use to study such problems. The PCE method will be employed in this work, see Appendix entitled ‘Polynomial Chaos Expansion’ for some introduction to the method to study sensitivity of damage rate prediction on uncertain system parameter  $\bar{\omega}$ .

Some studies which are of interest in the area of influence of uncertainties in flow and aeroelastic systems are discussed briefly here. Poirel and Price<sup>2</sup> have modeled and studied a structurally nonlinear aeroelastic system using linear aerodynamic theory subjected to gust loading conditions. Monte Carlo Simulations (MCS) were used to investigate the stochastic bifurcation behavior. Pettit et al.<sup>4</sup> have used horizontal and vertical gust models with an unsteady vortex lattice solver on a rigid flat plate. Further, Pettit and Beran<sup>5</sup> have studied the effects of parametric uncertainties on airfoil flutter limit cycle oscillation (LCO) using MCS. Desai and Sarkar<sup>6</sup> have modeled and studied a nonlinear aeroelastic system using a linear aerodynamic theory with structural uncertainties under a uniform wind and have given a comparison between standard MCS and PCE solutions. However studies of uncertainties of damage rate predictions is in its beginning. In our earlier work, Sarkar et al.<sup>7</sup> have studied the fatigue damage rate uncertainties for a simpler aeroelastic model of single degree-of-freedom torsional oscillation. Aerodynamic loads were estimated using semi-empirical method which is based on fitting load coefficients from experimental data. A stationary random gust was considered on the structure with its mean having a Gaussian variation. It was felt in the previous study that the effect of structural parameter uncertainty should also be taken into consideration. This is now

attempted in the present study. Also, the aeroelastic model is improved to take into account both pitch-plunge oscillations which is a more likely scenario in blades. The aerodynamic loads are calculated by both analytical and computational techniques and are more accurate.

## Fatigue Damage Criteria

Fatigue damage of a material takes place when the the material is subjected to repeated loading and unloading. Most often constant amplitude periodic loads are used to study the resistance of the material to fatigue damage which is measured by the number of periods it takes for a failure. These results are then represented in the form of S-N (stress vs. number of cycles) curve, also called as Wöhler curve. However the real loads encountered in actual practice are seldom a constant amplitude load. Hence there is a need to follow a cycle counting procedure which reduces the varying stress data into a set of cycles that allows for the application of damage rules in order to assess the fatigue life of the structure.

Yang and Fatemi<sup>8</sup> have given a detailed account of different damage rules in use today. Though many fatigue models have been developed, none of them are universally accepted. Each model accounts for only a limited number of cases where it works satisfactorily. In the present work, as is often done in engineering, the linear fatigue damage rule commonly known as Palmgren-Miner's rule<sup>9:10</sup> which defines a damage  $D$  as

$$D = \sum_{n=1}^k \frac{n_i}{N_i} \quad (1)$$

From Eq. (1),  $N_i$  is the number of cycles to failure when a constant amplitude reversible load of  $S_i$  is acting;  $n_i$  is the actual number of cycles over which the constant amplitude reversible load of  $S_i$  is acting and  $k$  is the number of stress blocks. For variable amplitude loads  $n_i$  is the number of rainflow cycles having range  $S_i$  counted in the load. Here local definition of rain-flow cycles, proposed in<sup>11</sup>, will be used. The fatigue failure is predicted when the damage  $D$  exceeds one, or some smaller threshold.

Often the environmental loads can be modeled as a sequence of stationary conditions resting for a period  $T$ , say. If the mean stress between the stationarity periods are approximately equal and  $T$  sufficiently long then the

stress ratio

$$d = D/T,$$

can be considered constant and the total damage due to  $N$  stationary load conditions are  $D \approx NT E[d]$  where expected damage rate is computed using the long-term distribution of wind spectra parameters for structure location. In this paper we shall study uncertainty of the damage  $D$  accumulated over a period of  $T = 120$  seconds.

More precisely damage rate will be computed in three cases: in the first one only the stresses due to torsion are considered; in the second stresses due to bending are used and in the third method combines the two ones by means of ‘equivalent’ uniaxial sign von Mises stress<sup>12</sup> where sign of the stress is defined by the highest principal stress. ( The stress calculation for the bending and torsion modes are discussed in detail in Appendix 3. )

Finally, as a representative material, Aluminum alloy 6082-T6 is considered here to compare the fatigue damage between the analytical and UVLM models. Experimental data have been analyzed and presented in an earlier work<sup>13</sup> (second chapter), which is used to estimate the fatigue life of Al 6082-T6 in bending and torsion. S-N relationship for these (bending and torsion data) are fitted in the form of  $N = CS^b$  with the given data to estimate damage. The fitted behavior is shown in Appendix 3. The present work incorporates the WAFO toolbox for rain-flow counting and the evaluation of damage<sup>14</sup>.

## Governing Equations of Motions

Fig. 1 shows a schematic plot of the two degrees-of-freedom (2D) classical pitch-plunge (bending-torsion) aeroelastic system. The equations of motion for the structurally linear system have been derived in<sup>15</sup>. With nonlinear restoring forces such as with cubic springs in both pitch and plunge, the equations of motion can be written as,

$$\begin{aligned} m\ddot{h} + S_a\ddot{\alpha} + 2c_h\dot{h} + K_h h + K_{h_1} h^3 &= L_\alpha \\ S_a\ddot{h} + I_\alpha\ddot{\alpha} + 2c_\alpha\dot{\alpha} + K_\alpha\alpha + K_{\alpha_1}\alpha^3 &= M_\alpha \end{aligned} \quad (2)$$

The above equation in the nondimensional form is given as<sup>1</sup>,

$$\begin{aligned}
\varepsilon'' + x_\alpha \alpha'' + 2\zeta_\varepsilon \frac{\bar{\omega}}{U} \varepsilon' + \left(\frac{\bar{\omega}}{U}\right)^2 (\varepsilon + \beta_\varepsilon \varepsilon^3) &= -\frac{1}{\pi\mu} C_L(\tau) \\
\frac{x_\alpha}{r_\alpha^2} \varepsilon'' + \alpha'' + 2\frac{\zeta_\alpha}{U} \alpha' + \frac{1}{U^2} (\alpha + \beta_\alpha \alpha^3) &= \frac{2}{\pi\mu r_\alpha^2} C_M(\tau)
\end{aligned} \tag{3}$$

where  $\zeta_\alpha$  and  $\zeta_\varepsilon$  are structural damping ratios in pitch and plunge respectively,  $\beta_\alpha$  and  $\beta_\varepsilon$  denote coefficients of cubic spring in pitch and plunge respectively. Among other nondimensional structural parameters,  $x_\alpha$  is the first moment of inertia and  $r_\alpha$  is the radius of gyration,  $\bar{\omega}$  is the natural frequency ratios of plunge and pitch degrees-of-freedom. In the following work, the parameter  $\bar{\omega}$  will be considered as uncertain.

## Analytical Model for $C_L$ and $C_M$ in (3)

Here we consider the classical formulation given by Wagner<sup>1</sup> in which the airfoil is approximated as a flat plate and the unsteady wake is assumed to be fixed to the body. For incompressible, inviscid flow, with small amplitude of oscillation of the body, the expressions for unsteady lift ( $C_L(\tau)$ ) and pitching moment coefficients ( $C_M(\tau)$ ) respectively can be analytically modeled in the time domain using the classical approach of Wagner<sup>15</sup>. The unsteady loads are expressed in the form of Duhamel's integrals in terms of a time domain function called Wagner function<sup>15</sup>. This analytical approach models the body as a zero thickness flat plate and also assumes the unsteady wake to be rigidly attached to the body's trailing edge.

The integral form of the loads at the right hand side makes the direct integration of the governing differential equations difficult. To solve this integro-differential form, four new variables  $w_1, w_2, w_3, w_4$  were introduced<sup>1</sup>, thus reformulating the equations in the following first order form,

$$\mathbf{x}' = f(\mathbf{x}, \text{system parameters}). \tag{4}$$

Here,  $\mathbf{x}$  is an array of eight variables as given below:

$$\{x_1, x_2, x_3, x_4, x_5, x_6, x_7, x_8\} = \{\alpha, \alpha', \varepsilon, \varepsilon', w_1, w_2, w_3, w_4\}. \tag{5}$$

More for details on this formulation, the readers are referred to Appendix 1.

## $C_L$ and $C_M$ Estimated by Means of Unsteady Vortex Lattice Method

Subsequently, an unsteady potential flow solver based on a 2D unsteady vortex lattice method (UVLM) is implemented to calculate the aerodynamic loads at the right hand side of the governing equations, i.e.  $C_L$  and  $C_M$ . In contrast to classical approach here the wake is free to evolve with its own local velocities. This method discretizes the actual shape of the body and the wake into computational elements. In the present work, the unsteady Hess and Smith panel method is implemented<sup>16</sup> and is used for the time dependent load calculations.

The airfoil surface is divided into a number of small segments called panels. The body is represented using two types of singularity elements, sources and vortices. The velocity at any point  $(x,y)$  in the flow-field is vector sum of velocity of undisturbed flow (free stream) and disturbance field due to the presence of the oscillating body and the wake behind the body. The wake behind the airfoil also consists of discretized elements. The boundary condition that the surface of the body is a streamline of the flow is satisfied by taking the summation of velocities induced by body bound singularities, free-stream and wake vortices to be equal to zero in the direction normal to the surface at each panel. The source singularity strength is considered to be constant over a particular panel and the vorticity strength is considered to be constant over all the panels and their values are computed using the boundary condition and also the Kutta condition. Kutta condition is imposed to ensure smooth flow at the trailing edge. For inviscid flow, Kelvin's theorem states that the total circulation in the flow-field must be preserved and that any changes in the circulation about the body is balanced by an equal and opposite vorticity added in the wake. These shed vortices influence the local velocity field significantly and as a result the forces on the airfoil at any instant are influenced by the past motion of airfoil. All the wake vortices are shed from the trailing edge of the airfoil. In unsteady potential flow, the calculation of pressure at any point on the body is done by the use of unsteady Bernoulli's equation<sup>16</sup>.

The qualitative flow-field for a sinusoidally oscillating NACA 0012 airfoil with its evolving wake pattern behind the trailing edge is shown in Fig. 2. The shape of the wake is dictated by the local velocities of the wake vorticity elements. Hence the name, free wake model in contrast to the rigid wake

model of analytical method in which the wake moves with the free-stream<sup>17</sup>. UVLM also accounts for the airfoil geometry; the effect of airfoil shape and thickness is significant on the wake pattern which finally affect the unsteady aerodynamic loads.

## Simulation of Gust Time Histories

The simulation of gust time histories is done by using the approach given by<sup>18</sup>. The von Karman spectral density has been used in the present simulation to model the horizontal gust fluctuations<sup>4</sup>.

$$S_{uu}(\omega) = \frac{2\sigma_u^2 L_u}{\pi V_\infty} \frac{1}{[1 + (1.339 L_u \omega / V_\infty)^2]^{5/6}}, \quad 0.01 \leq \omega \leq 40 \quad (6)$$

$V_\infty$  is the mean wind at 6.1 m/s and the following gust parameter values have been considered in the present study,  $\sigma_u = 0.52303$  m/s;  $L_u = 152.5$  m. The vertical component of the gust is assumed to be absent. Simulation of horizontal fluctuations  $u(t)$ , from its spectral density function is done by superimposing a set of sinusoidal components.

$$u(t) = \sum_{n=1}^{N_w} \sqrt{2S_{uu}(\omega_n)\Delta\omega_n(\omega_n)} \cos(\omega_n t + \phi_n) \quad (7)$$

$\phi_n$ s are uniformly distributed random variables between 0 and  $2\pi$  and  $N_w = 1000$ . It is well known that Gaussian process possessing PSD is ergodic. Since  $u(t)$  is an approximation of the ergodic Gaussian process, approximately, the average quantity like damage, will converge to the ensemble mean of the quantity. Hence basically one sequence of the random phases is needed to estimate damage rate dependence on uncertain parameters. In the present work, the focus is on estimating average quantities like rate of damage over a long time simulation, and hence this assumption. A PCE formulation is done for the structural parameter  $\bar{\omega}$  which is considered to be a Gaussian random variable with mean = 0.2 and coefficient of variation = 5%. Sensitivity of the fatigue damage on this structural parameter variation is shown in a later section.

## Validation of the UVLM Code and Aeroelastic Response

A validation of the UVLM aerodynamic model has been done with the earlier results of Young<sup>17</sup> for both computational and analytical results. They are compared in terms of the peak lift and moment coefficients for a rigid airfoil driven in plunge and the results have matched quite well as shown in Fig. 3 (a),(b). The analytical approach over predicts the load and this difference increases with the frequency.

Ensuring that the code is working fine in the flow only part, the next step was to couple the structural part with it. In this step, the lift coefficient obtained from the flow part is substituted in Eq. (2), and the position of the airfoil is updated at each time step. A symmetric NACA 0012 airfoil profile has been used in the aerodynamic model. The structural parameters are:  $\mu = 41.3833$ ;  $x_\alpha = 0.33586$ ;  $r_\alpha = 0.57378$ ;  $\beta_\alpha = 3$ ;  $\beta_\varepsilon = 0$ ;  $b = 0.5\text{m}$  and  $\bar{\omega} = 0.2$ .

It was seen that the linear flutter speed predicted by both UVLM and analytical calculations are reasonably close and are in good agreement with each other in the above chosen parameter ranges. The non-dimensional critical speed (flutter) predicted by UVLM is 4 while that predicted by the analytical model is 4.29. The difference in the flutter speed can be attributed to the airfoil shape and the free wake aerodynamic model used in UVLM. UVLM considers a wake model in which the trailing edge wake is free to develop while the analytical model considers a Wagner's model<sup>15</sup> in which the wake is rigid and bound to the body. Also the airfoil geometry is taken into consideration in UVLM whereas the Wagner's model makes simplifications by neglecting the thickness and camber of the profile. Fig. 4 shows a qualitative comparison of the aeroelastic response under a sample gust realization for both UVLM and analytical model. Under the influence of same gust profile, the analytical formulation predicts higher amplitude of oscillation compared to UVLM.

## Sensitivity of Fatigue Damage on Structural Parameter $\bar{\omega}$

In Sarkar et al.<sup>7</sup>, a PCE relation between fatigue damage rate and average wind speed  $V_\infty$  has been presented. There, the aerodynamic load was simplified so as to consider the blade torsion only. Since the oscillation problem involved large angles of attack, viscous effects were included and the aerodynamic load was calculated using a semi-empirical model<sup>19</sup> (Onera model for dynamic stall). In the present case, loading in both torsion and bending are considered, however, here the viscous effects are not important hence load calculation can be done with analytical formulations. For higher accuracy and improved unsteady effects, UVLM is also used. Three formulas for damage accumulation will be compared; damage solely due to torsion then bending and multiaxial approach using equivalent signed von Mises stress, see Fig. 5 for a typical record of von Mises stress evaluated for the rotor blade. (The multi-axial state of stress time histories arising from the bending and torsion of a rotor blade is discussed at some details in Appendix 3.)

Summarizing, there are three damage rates considered for two models of loadings; the classical analytical formulation given by Wagner<sup>1</sup> and UVLM. This gives six damage rates. Sensitivity of the damage rates on structural parameter ( $\bar{\omega}$ ) is presented in Fig. 6. We can see that the damage rate is very sensitive for the value of the  $\bar{\omega}$  growing by factor two for the considered cases.

## Uncertainty in Fatigue Damage Prediction

Fig. 7 show damage PDFs ( $T= 120$  secs) for equivalent signed von Mises, torsion and bending situations for two models of environmental load, i.e. six cases. The variability of damage rates caused by uncertainty of  $\bar{\omega}$  is described by means of the pdf's. Note that  $\bar{\omega}$  is considered as normally distributed random variable with mean 0.2 and standard deviation 0.01.

First of all, as is mentioned in Appendix 3, the torsion stress is much larger than the bending stress so we expect that damage computed for solely torsion and von Mises stress should be much higher than the damage rate computed for bending originated stresses. This is also the case as can be seen in plots shown in Fig. 7. We conclude that for system considered neglecting torsion in fatigue damage prediction would lead to gross errors. Secondly one can see

that modeling error can also be very large. We can see that using analytical description of environmental loads will give damage rates between two and three times larger than the damage rates evaluated for UVLM model. There is also non negligible uncertainty due to choice of fatigue criterion based solely on torsion stresses and the equivalent multiaxial signed von Mises stress. The damage rates for the multiaxial fatigue criterion are about 25% higher for the chosen system.

Summarizing in our study the largest uncertainties in fatigue damage predictions are due to choice of the model to describe environmental load. Variability due to uncertainty in the value of parameter  $\bar{\omega}$ , the natural frequency ratio in plunge and pitch, is of similar size. Finally, for the chosen system, uncertainty on selection of fatigue damage criterion, uniaxial or multiaxial is much smaller but not negligible.

## Summary & Conclusions

A nonlinear flutter model of a model rotor blade with different sources of uncertainty has been considered in the present study. The unsteady aerodynamic loads are calculated for the bending-torsion oscillation model of blade section. The system is subjected to horizontal gust, modeled as a stationary process. Different sources of uncertainty are investigated for their relative effect on the fatigue damage estimate of the blade. This is a qualitative comparison of their effect on the model blade rather than a quantitative life prediction of an actual rotor. Uncertainty in the structural stiffness parameter is assumed with a Gaussian variation and modeled using polynomial chaos expansion (PCE). PCE needs to use smaller number of deterministic runs compared to Monte Carlo samples. Modeling error uncertainty is another important source of uncertainty in predicting the aeroelastic stability boundary (flutter) and also the fatigue life. Two different aeroelastic models, using two different unsteady inviscid flow solvers have been compared; an analytical flow model and a two dimensional vortex lattice code. The analytical model approximates the airfoil as a thin flat plate with the unsteady wake rigidly attached to it. The vortex lattice method takes into account the shape of the airfoil and also evolution of the wake pattern, hence based on a more realistic unsteady flow situation than the analytical model. The damage pattern is similar but damage values are higher with the analytical model. Thus, the analytical model is seen to be more conservative. There is

a significant computational advantage is using the analytical model as well, as the higher fidelity UVLM code takes much longer to run. For fatigue life estimate, three different criteria based on torsion, bending and multiaxial stress are used. Multiaxial stress situation is converted to an equivalent uniaxial case using a signed von Mises criterion. The damage patterns for von Mises and torsion were close to each other. The effect of bending is much smaller compared to torsion, but not entirely absent. Thus the uncertainty on the choice of fatigue criteria is smaller compared to the other sources of uncertainty, though not entirely negligible.

## References

- [1] Lee, B., Jiang, L., and Wong, Y. (1998) Flutter of an airfoil with cubic nonlinearity restoring force. *AIAA J*, **1725**, 237–257.
- [2] Poirel, D. and Price, S. J. (2007) Bifurcation characteristics of a two-dimensional structurally non-linear airfoil in turbulent flow. *Nonlinear Dynam*, **48**, 423–435.
- [3] Ghanem, R. G. and Spanos, P. (1991) *Stochastic Finite Elements: a Spectral Approach*. Springer-Verlag.
- [4] Pettit, C., Hajj, M., and Beran, P. (2010) A stochastic approach for modeling incident gust effects on flow quantities. *Probabilist Eng Mech*, **25**, 153–162.
- [5] Pettit, C. L. and Beran, P. S. (2003) Effects of parametric uncertainty on airfoil limit cycle oscillation. *J Aircraft*, **40**, 1004–1006.
- [6] Desai, A. and Sarkar, S. (2010) Analysis of a nonlinear aeroelastic system with parametric uncertainties using polynomial chaos expansion. *Math Probl Eng*, **2010**, 1–21.
- [7] Sarkar, S., Gupta, S., and Rychlik, I. (2010) Wiener chaos expansions for estimating rain-flow fatigue damage in randomly vibrating structures with uncertain parameters. *Probabilist Eng Mech*, **26**, 387–398.
- [8] Yang, L. and Fatemi, A. (1998) Cumulative fatigue damage and life prediction theories: A survey of the state of the art for homogeneous materials. *Int J Fatigue*, **20**, 9–34.

- [9] Palmgren, A. (1924) Die lebensdauer von kugellagern. *VDI Zeitschrift*, **68**, 339–341.
- [10] Miner, M. A. (1945) Cumulative damage in fatigue. *J Appl Mech*, **12**, A159–A164.
- [11] Rychlik, I. (1987) A new definition of the rainflow cycle counting method. *Int J Fatigue*, pp. 119–121.
- [12] Bracessi, C., Cianetti, F., Lori, G., and Pioli, D. (2008) An equivalent uniaxial stress process for fatigue life estimation of mechanical components under multiaxial stress conditions. *Int J Fatigue*, **30**, 1479–1497.
- [13] Carpinteri, A., de Freitas, M., and Spagnoli, A. (2003) *Biaxial/Multiaxial Fatigue and Fracture*. Elsevier,ESIS Publication.
- [14] Brodtkorb, P., Johannesson, P., Lindgren, G., Rychlik, I., Rydén, J., and Sjö, E. (2000) WAFO - a Matlab Toolbox for the Analysis of Random Waves and Loads. *Proc. 10'th Int. Offshore and Polar Eng. Conf., ISOPE, Seattle, USA*, vol. 3, pp. 343–350.
- [15] Fung, Y. C. (1955) *An Introduction to the Theory of Aeroelasticity*. John Wiley & Sons, Inc.
- [16] Cebeci, T., Platzer, M., Chen, H., Chang, K.-C., and Shao, J. P. (2004) *Analysis of Low-Speed Unsteady Airfoil Flows*. Horizons Publishing.
- [17] Young, J. (2005) *Numerical simulation of the unsteady aerodynamics of flapping airfoils*. Ph.D. thesis, School of Aerospace, Civil and Mechanical Engineering, The University of New South Wales.
- [18] Shinozuka, M. and Jan, C. (1972) Digital simulation of random processes and its applications. *J Sound Vib*, **25**, 111–128.
- [19] Tran, C. T. and Petot, T. (1981) Semi-empirical models for dynamic stall of airfoils in view of the application to the calculation of responses of a helicopter blade in forward flight. *Vertica*, **5**, 35–53, (Also published in ONERA TP, no. 1980–103, 1980).
- [20] Jones, R. T. (1940) The unsteady lift of a wing of finite aspect ratio. Tech. Rep. 681, NACA Report.

- [21] Cameron, R. H. and Martin, W. T. (1947) The orthogonal development of nonlinear functionals in series of Fourier-Hermite functionals. *Ann Math*, **48**, 385–392.
- [22] Xiu, D. and Karniadakis, G. E. (2003) Modelling uncertainty in flow simulations via generalized polynomial chaos. *J Comput Phys*, **187**, 137–167.
- [23] Witteveen, J. A. S., Sarkar, S., and Bijl, H. (2007) Modeling physical uncertainties in dynamical stall induced fluid structure interaction of turbine blades using arbitrary polynomial chaos. *Comput Struct*, **85**.
- [24] Xiu, D., Lucor, D., Su, C.-H., and Karniadakis, G. E. (2002) Stochastic modeling of flow-structure interactions using generalized polynomial chaos. *J Fluid Eng-T ASME*, **124**, 51–59.
- [25] Millman, D. R., King, P. I., and Beran, P. S. (2003) A stochastic approach for predicting bifurcation of a pitch and plung airfoil. *21<sup>st</sup> AIAA Applied Aerodynamics Conference*, Orlando, FL, AIAA-2003-3515.
- [26] Pettit, C. L. and Beran, P. S. (2006) Spectral and multiresolution Wiener expansions of oscillatory stochastic process. *J Sound Vib*, **294**, 752–779.
- [27] Millman, D. R. (2004) *Quantifying initial conditions and parametric uncertainties in a nonlinear aeroelastic system with an efficient stochastic algorithm*. Ph.D. thesis, Air force Institute of Technology, Wright-Patterson Airforce Base, Ohio.
- [28] Megson, T. (2005) *Structural And Stress Analysis*. Elsevier, second edn.
- [29] Timoshenko, S. and Goodier, J. N. (1951) *Theory of Elasticity*. McGraw-Hill.

## APPENDIX 1

### Analytical Model for Aerodynamic Loads

For incompressible, inviscid flow, the unsteady lift and pitching moment coefficients,  $C_L(\tau)$  and  $C_M(\tau)$  can be written analytically in terms of the Wagner function  $\phi(\tau)$ <sup>15</sup> as (please note that  $\phi$  is used as a standard notation and is different from any other  $\phi$  that have been used elsewhere in the paper outside this Appendix).

$$C_L(\tau) = \pi \{ \varepsilon''(\tau) - a_h \alpha''(\tau) + \alpha'(\tau) \} + 2\pi \left\{ \alpha(0) + \varepsilon'(0) + \left[ \frac{1}{2} - a_h \right] \alpha'(0) \right\} \phi(\tau) \\ + 2\pi \int_0^\tau \phi(\tau - \sigma) \left[ \alpha'(\sigma) \varepsilon''(\sigma) + \left[ \frac{1}{2} - a_h \right] \alpha''(\sigma) \right] d\sigma \quad (8)$$

$$C_M(\tau) = \pi \left[ \frac{1}{2} + a_h \right] \times \left\{ \alpha(0) + \varepsilon'(0) + \left[ \frac{1}{2} - a_h \right] \alpha'(0) \right\} \phi(\tau) \\ + \pi \left[ \frac{1}{2} + a_h \right] \int_0^\tau \phi(\tau - \sigma) \left\{ \alpha'(\sigma) + \varepsilon''(\sigma) + \left[ \frac{1}{2} - a_h \right] \alpha''(\sigma) \right\} d\sigma \\ + \frac{\pi}{2} a_h \{ \varepsilon''(\tau) - a_h \alpha''(\tau) \} - \left[ \frac{1}{2} - a_h \right] \frac{\pi}{2} \alpha'(\tau) - \frac{\pi}{16} \alpha''(\tau) \quad (9)$$

The Wagner function  $\phi(\tau)$  in terms of the nondimensional time is given by:

$$\phi(\tau) = 1 - \psi_1 e^{-\epsilon_1 \tau} - \psi_2 e^{-\epsilon_2 \tau} \quad (10)$$

Values for the constants are,  $\psi_1 = 0.165$ ,  $\psi_2 = 0.335$ ,  $\epsilon_1 = 0.0455$  and  $\epsilon_2 = 0.3$ <sup>20</sup>. Introducing the following new variables  $w_1, w_2, w_3, w_4$ , the original integro-differential equations for aeroelastic system given by Eq.3 can be reformulated<sup>1</sup>.

$$w_1 = \int_0^\tau e^{-\epsilon_1 (\tau - \sigma)} \alpha(\sigma) d\sigma$$

$$w_2 = \int_0^\tau e^{-\epsilon_2 (\tau - \sigma)} \alpha(\sigma) d\sigma$$

$$w_3 = \int_0^\tau e^{-\epsilon_1 (\tau - \sigma)} \varepsilon(\sigma) d\sigma$$

$$w_4 = \int_0^\tau e^{-\epsilon_2 (\tau - \sigma)} \varepsilon(\sigma) d\sigma$$

The above expressions give way to the following:

$$\begin{aligned}w'_1 &= \alpha - \epsilon_1 w_1 \\w'_2 &= \alpha - \epsilon_2 w_2 \\w'_3 &= \varepsilon - \epsilon_1 w_3 \\w'_4 &= \varepsilon - \epsilon_2 w_4\end{aligned}$$

Now a set of autonomous first order forms are obtained as follows:

$\mathbf{x}' = f(\mathbf{x})$  are obtained as,  $\mathbf{x} = \{x_1, x_2, x_3, x_4, x_5, x_6, x_7, x_8\} = \{\alpha, \alpha', \varepsilon, \varepsilon', w_1, w_2, w_3, w_4\}$ .

Explicitly, the system looks like,

$$\begin{aligned}x'_1 &= x_2 \\x'_2 &= (c_0 N - d_0 M)/(c_1 d_0 - c_0 d_1) \\x'_3 &= x_4 \\x'_4 &= (-c_1 N + d_1 M)/(c_1 d_0 - c_0 d_1) \\x'_5 &= x_1 - \epsilon_1 x_5 \\x'_6 &= x_1 - \epsilon_2 x_6 \\x'_7 &= x_3 - \epsilon_1 x_7 \\x'_8 &= x_3 - \epsilon_2 x_8,\end{aligned}\tag{11}$$

where,

$$M = c_2 x_4 + c_3 x_2 + c_4 x_3 + c_5 x_3^3 + c_6 x_1 + c_7 x_5 + c_8 x_6 + c_9 x_7 + c_{10} x_8 - f(\tau)$$

$$N = d_2 x_2 + d_3 x_1 + d_4 x_1^3 + d_5 x_4 + d_6 x_3 + d_7 x_5 + d_8 x_6 + d_9 x_7 + d_{10} x_8 - g(\tau)$$

The values of  $c_0 \dots c_{10}, d_0 \dots d_{10}, f(\tau)$  and  $g(\tau)$  depend on the system parameters<sup>1</sup>.

## APPENDIX 2

### Polynomial Chaos Expansion

System response  $X(t, \theta)$  is defined in a probability space given by  $(\Omega, \mathcal{A}, P)$ , with  $\theta \in \Omega$ .  $X(t, \theta)$ , which is second order stationary, can be written as<sup>21</sup>:

$$X(t, \vec{\xi}) = \sum_{j=0}^{\infty} a_j(t) \Phi_j(\vec{\xi}(\theta)) \quad (12)$$

where polynomials  $\Phi_j$  forms a basis and  $\vec{\xi} = \xi_1, \xi_2, \dots$  are random variables defined on the probability space. The choice of the basis function depends on the random variables  $\vec{\xi}$ . In the original form, Gaussian random variables were used and  $\Phi_j$ s were Hermite polynomials. The basis polynomials are chosen so as to be orthogonal with respect to  $\mathcal{P}_{\vec{\xi}}$  and the speed of convergence depends on the choice of basis. The first few one-dimensional ( $\xi_1$ ) Hermite polynomials are given as:

$$\begin{aligned} \Phi_0(\xi_1) &= 1, \\ \Phi_1(\xi_1) &= \xi_1, \\ \Phi_2(\xi_1) &= \xi_1^2 - 1, \\ \Phi_3(\xi_1) &= \xi_1^3 - 3\xi_1, \\ \Phi_4(\xi_1) &= \xi_1^4 - 6\xi_1^2 + 3, \end{aligned}$$

Other Hermite polynomials can be generated from the following recurrence relationship,

$$\Phi_n(\xi_1) = \xi_1 \Phi_{n-1} - (n-1) \Phi_{n-2}.$$

However, the exponential convergence of the polynomial chaos expansion has been extended to several other types of commonly used probability distributions. One can use orthogonal polynomials from the generalized Askey scheme for some standard non-Gaussian input uncertainty distributions such as gamma and beta as given in<sup>22</sup>. For any arbitrary input distribution, a Gram-Schmidt orthogonalization can be employed to generate the orthogonal family of polynomials given by<sup>23</sup>. Any stochastic process  $\alpha(t, \vec{\xi})$ , governed by Gaussian random variables  $\vec{\xi}$  ( $\vec{\xi}$  can always be normalized as standard Gaussian) can then be approximated by the following truncated series:

$$\alpha(t, \vec{\xi}) \approx \sum_{j=0}^p \hat{\alpha}_j(t) \Phi_j(\vec{\xi}(\theta)) \quad (13)$$

Note that, here the infinite upper limit of Eq. (12) is replaced by  $p$ , called the order of the expansion. For multi-dimensional random variables ( $n$ ), with number of polynomial terms denoted by  $n_p$ , the minimum value is given by

the following<sup>24</sup>.

$$p = \frac{(n + n_p)!}{n!n_p!} - 1 \quad (14)$$

A number of non-intrusive variants of PCE have been developed to counter the disadvantages of the classical Galerkin method. Stochastic projection is one of them<sup>3;25</sup>. In the present study, a stochastic projection based approach is used to evaluate the chaos coefficients. Here, the chaos expansions are not substituted in the governing equations; instead samples of the solutions are used (using a low order pseudo-Monte Carlo method) to evaluate the coefficients directly using a projection formula. As a result, this approach can utilize the existing deterministic code and hence the name non-intrusive. The random process is approximated by a truncated series, as shown in Eq. (13).

The Hermite polynomials are statistically orthogonal, that is, they satisfy  $\langle \Phi_i, \Phi_j \rangle = 0$  for  $i \neq j$ , hence the expansion coefficients can be directly evaluated as:

$$\hat{\alpha}_j(t) = \frac{\langle \alpha(t, \vec{\xi}), \Phi_j \rangle}{\langle \Phi_j^2 \rangle} \quad (15)$$

The denominator in Eq. (15) can be shown to satisfy  $\langle \Phi_j^2 \rangle = j!$  for non-normalized Hermite polynomials<sup>26</sup>. So the key step in projecting  $\alpha(t, \theta)$  along the polynomial chaos basis is the evaluation of  $\langle \alpha, \Phi_j \rangle$ .

For a single random variable case ( $\xi_1$ ),

$$\langle \alpha(t, \xi_1), \Phi_k(\xi_1) \rangle = \int_{-\infty}^{+\infty} \alpha(t, \xi_1), \Phi_k(\xi_1) \phi(\xi_1) d\xi_1 \quad (16)$$

Where the weighting function  $\phi(\xi_1)$  is the Gaussian probability density function. For zero mean and unit variance case, this is given by the following,

$$\phi(\xi_1) = \frac{1}{\sqrt{2\pi}} e^{-\frac{1}{2}\xi_1^2} \quad (17)$$

The evaluation of  $\langle \alpha(t, \xi_1), \Phi_k \rangle$  is done by using a Gauss-Hermite quadrature numerical integration scheme. The quadrature points along  $\xi_1$  are taken as the equi-probability points (for the definition of equi-probability points, see<sup>27</sup>). At these points, the corresponding samples of the uncertain parameter is used to run the pseudo-MCS. The realizations of the system response  $\alpha(t, \xi_1)$  are then used to estimate the deterministic coefficients,  $\hat{\alpha}_j(t)$ s in Eq. (15).

## APPENDIX 3

### Stress Calculation and Damage

The turbine blade is assumed to be a cantilever beam with the same airfoil cross-section throughout its length. The blade is assumed to undergo torsion (airfoil pitching) and bending (airfoil plunging). The centrifugal stresses caused due to the rotation of the blade has not been taken into consideration and only the shear stresses and bending stresses caused due to torsion and bending have been considered. The turbine blade has been assumed to be made of aluminum alloy Al 6082-T6 with modulus of elasticity  $E = 70$  GPa, the shear modulus  $G = 26.4$  GPa. The SN characteristics for this material have been fitted from the data given in<sup>13</sup>, chapter 2, for bending and torsion. These are plotted in Fig. 8.

#### Stress calculation related to bending

The load and the corresponding stress on a cantilever beam is estimated in the following way. For the sake of simplicity it is assumed that, the beam is subjected to a uniformly distributed load. Megson<sup>28</sup> describes the plunge deflection at the tip of a cantilever beam under a uniformly distributed load to be,

$$\delta_{tip} = \frac{w_{uni}l^4}{8EI}, \quad (18)$$

where  $\delta_{tip}$  is the plunge deflection,  $I$  is the moment of inertia of the airfoil cross section,  $w_{uni}$  is the load per unit length of the blade,  $l$  is the length of the blade. The plunge deflection estimated from the airfoil model is assumed as the tip deflection.

The term  $w_{uni}l$  (called net loading) introduces a shear force as well as bending moment which in turn introduces normal stresses. The shear stress component  $\tau_{yz}$  due to the net loading is given in the following. The beam has its longitudinal axis along the  $z$  and vertical axis along the  $y$  directions respectively.

$$\tau_{yz} = \frac{PA\bar{y}}{Ic} \quad (19)$$

where  $P$  is the load  $= w_{uni}l$ ,  $A$  is the area above the neutral axis,  $\bar{y}$  is the centroid of the area and  $c$  is the width of the cross section. The plunge

deflection  $\delta_{tip}$  is time dependent, and so is the shear stress  $\tau_{yz}$ .

The load per unit length of the blade  $w_{uni}$  also produces a bending moment  $M$  which is given by  $(w_{uni}l^2)/2$ . The bending moment induces normal bending stress  $\sigma_{zz}$  in the beam.

$$\sigma_{zz} = \frac{My}{I} \quad (20)$$

where  $y$  is the height of the section above neutral axis. The bending stress  $\sigma_{zz}$  is maximum at  $y = y_{max}$  and the shear component  $\tau_{yz}$  near the neutral axis. However, in the present bending computations,  $\sigma_{zz}$  values are several magnitude larger than  $\tau_{yz}$  and thus this shear component is not taken into further calculations.

## Stress calculation related to torsion

Estimating the torsion stresses is not as straightforward as the bending case because of the unusual shape of the cross section involved. One needs to account for warping of the cross section as well. Prandtl's stress function approach is used here<sup>29</sup>. Let us assume a prismatic bar of arbitrary cross-section carrying a torsion couple  $T$  at the ends about the longitudinal  $z$  axis and passing through the centre of twist. The deformation of the twisted shaft consists of the rotations and warping of the cross sections.

Displacements due to rotation  $\Delta x$  and  $\Delta y$  in  $x$  and  $y$  directions respectively are given by,

$$\begin{aligned} \Delta x &= -r\beta \sin \alpha = -r\beta \frac{y}{r} = -yz\theta, \\ \Delta y &= r\beta \cos \alpha = r\beta \frac{x}{r} = xz\theta \end{aligned} \quad (21)$$

where,  $\beta = z\theta$  is the angle of rotation of the cross section at distance  $z$  along the blade. The cross section will also displace in the  $z$  direction as it warps out of the  $x - y$  plane. This warping displacement is assumed to be proportional to the rate of twist  $\theta$  and a function  $\psi(x, y)$  which describes the variation in  $\Delta z$  over the cross section<sup>29</sup>. This gives

$$\Delta z = \theta\psi(x, y) \quad (22)$$

From Eq. (21) and Eq. (22), it can be observed that the direct strains  $\epsilon_x = \frac{\partial \Delta x}{\partial x}$ ;  $\epsilon_y = \frac{\partial \Delta y}{\partial y}$  and  $\epsilon_z = \frac{\partial \Delta z}{\partial z}$  are all absent. Also  $\gamma_{xy} = \frac{\partial \Delta x}{\partial y} + \frac{\partial \Delta y}{\partial x} = 0$  which implies that cross section does not shear in the  $x$ - $y$  plane.

The strain components can be written as,

$$\gamma_{zx} = \frac{\partial \Delta x}{\partial z} + \frac{\partial \Delta z}{\partial x} = \theta \left( \frac{\partial \psi}{\partial x} - y \right) \quad (23)$$

$$\gamma_{zy} = \frac{\partial \Delta y}{\partial z} + \frac{\partial \Delta z}{\partial y} = \theta \left( \frac{\partial \psi}{\partial y} + x \right) \quad (24)$$

As a result, the stress components  $\sigma_x$ ,  $\sigma_y$ ,  $\sigma_z$  and  $\tau_{xy}$  would all be zero and shear stresses  $\tau_{zx} = G\gamma_{zx}$  and  $\tau_{zy} = G\gamma_{zy}$  would be present. Substituting the values, one would get,

$$\frac{\partial \tau_{zy}}{\partial x} - \frac{\partial \tau_{zx}}{\partial y} = 2G\theta \quad (25)$$

A stress function  $\phi$  called Prandtl stress function is introduced so as to satisfy,

$$\begin{aligned} \tau_{zx} &= \frac{\partial \phi}{\partial y} \\ \tau_{zy} &= -\frac{\partial \phi}{\partial x}. \end{aligned} \quad (26)$$

which give the following:

$$\frac{\partial^2 \phi}{\partial x^2} + \frac{\partial^2 \phi}{\partial y^2} = -2G\theta \quad (27)$$

Thus there are no normal stresses and the shear stresses are defined by components  $\tau_{zx}$  and  $\tau_{zy}$ .

In order to estimate the torsion stresses in an arbitrary cross section, the stress function should be known *a priori*. The stress function should be such that it satisfies Eq. 27 and also the boundary conditions. Timoshenko and Goodier<sup>29</sup> have given a generalized expression for  $\phi$  for airfoil-like section shapes. One can assume a polynomial fit for such cross section shapes as,

$$y = a\xi\left(\frac{x}{c}\right) \quad \text{and,} \quad y = -a_1\xi\left(\frac{x}{c}\right) \quad (28)$$

$$\text{with,} \quad \xi\left(\frac{x}{c}\right) = \left(\frac{x}{c}\right)^m \left[1 - \left(\frac{x}{c}\right)^p\right]^q \quad (29)$$

The parameters  $a, a_1, m, p, q$  are fitted according to the chosen cross section. The stress function is given in the following generalized form:

$$\phi = A(y - a\xi)(y + a_1\xi) \quad (30)$$

Here,  $A$  can be estimated in terms of  $G\theta$ ,  $a$ ,  $a_1$ , and  $\xi$ , as follows:

$$A = \frac{-G\theta}{1 + \alpha(a^2 + a_1^2 + aa_1)/c^2}, \quad (31)$$

where,  $\alpha = f(\xi)$ . Once  $\phi$  is known, the stress components can be estimated following Eq. 26. In the present study, a NACA 0012 symmetric airfoil has been assumed. For this, the parameters are fitted as:  $a = a_1 = 0.94$ ,  $m = 0.75$ ,  $p = 0.139$ ,  $q = 1$ ,  $\alpha = 0.0083$ . The airfoil profile is reproduced using these values and plotted along with a NACA 0012 profile (Fig. 9) and the match is excellent.

The blade is assumed to be a standard rotor blade of length 20 m and the chord length is assumed to be 1 m. Maximum  $\tau_{xz}$  occurs at  $y = y_{\max}$  and maximum  $\tau_{yz}$  near the leading edge. However,  $\tau_{xz}$  values are larger than  $\tau_{yz}$  at least by one order of magnitude. Finally, the most significant stress components from both bending and torsion are found to be  $\sigma_{zz}$  and  $\tau_{xz}$ . A typical case of stress time histories are plotted in Fig. 10. Damage calculations are done based on these stress components individually and also on an equivalent uniaxial stress using the signed von Mises criteria.

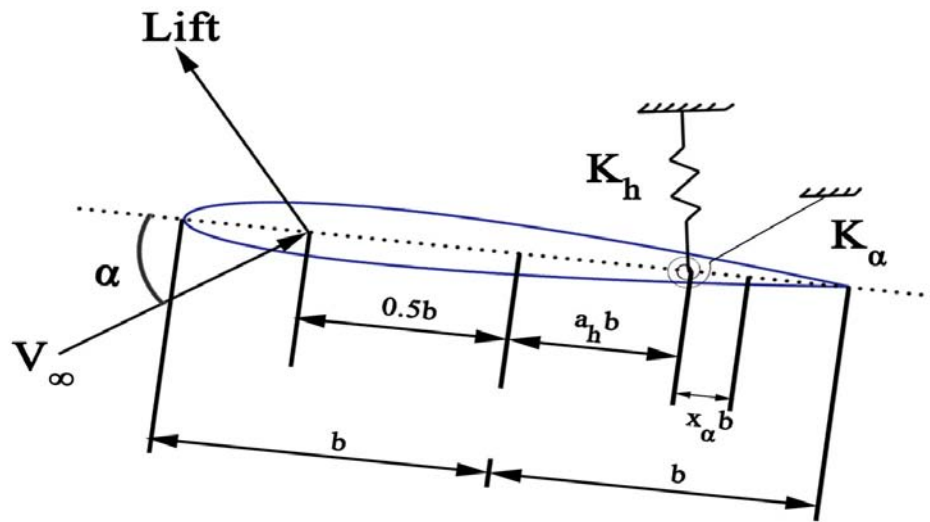


Figure 1: The schematic of a symmetric airfoil with pitch and plunge degrees-of-freedom.

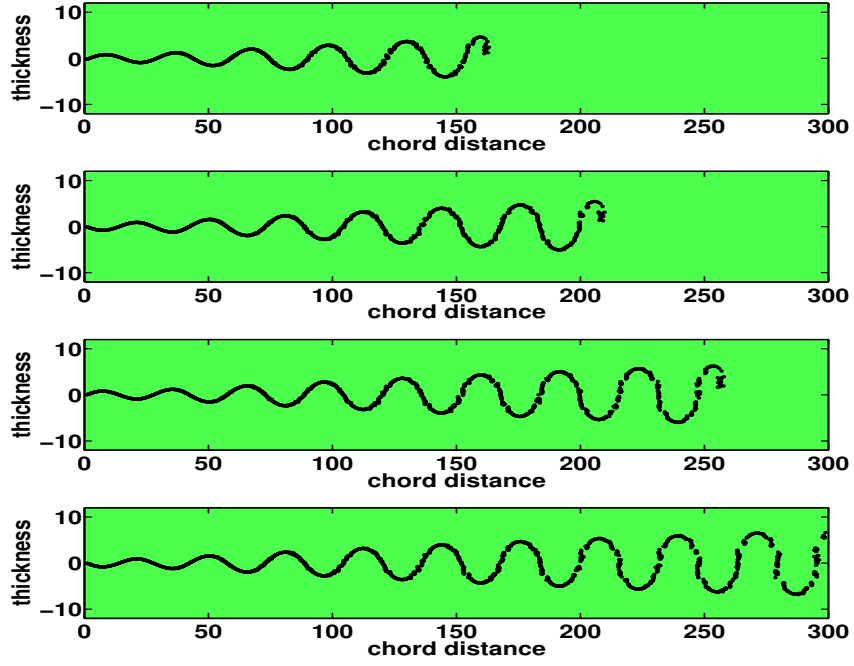
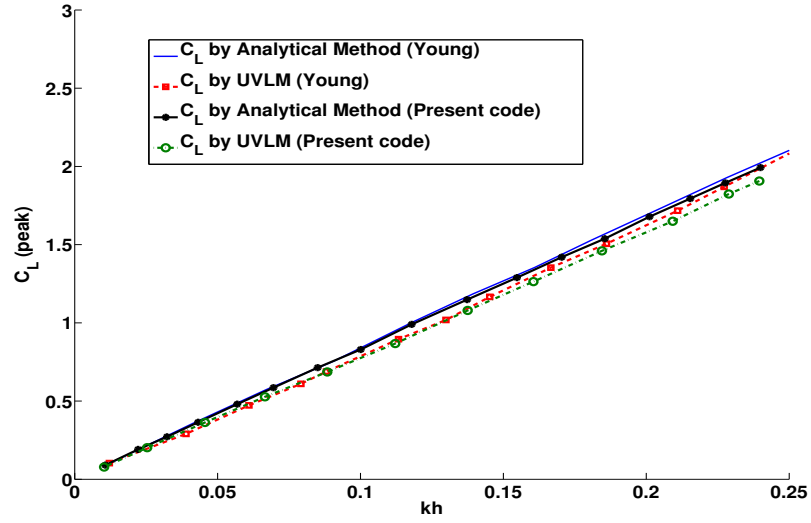
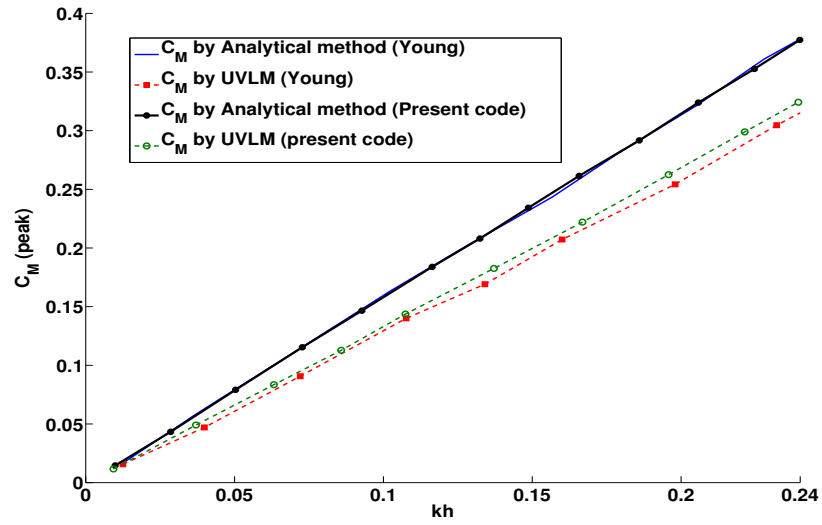


Figure 2: Freely developing wake behind an oscillating NACA 0012 simulated with UVLM at various time instances.



(a)



(b)

Figure 3: UVLM vs. analytical results<sup>17</sup>, (a) peak lift coefficient, (b) peak moment coefficient.

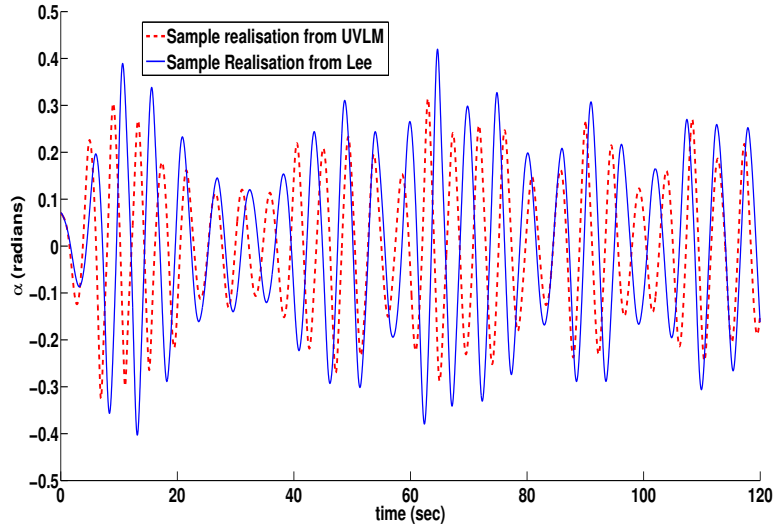


Figure 4: Comparison of a sample realization under gust : UVLM and analytical method.

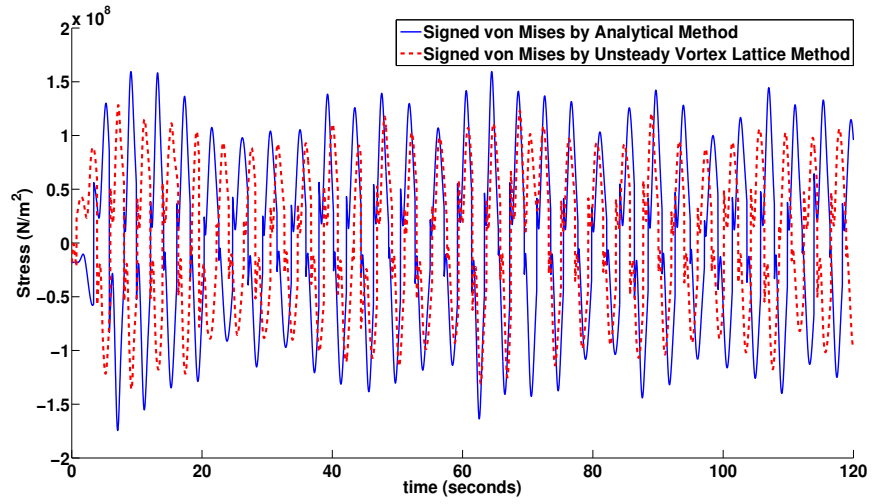
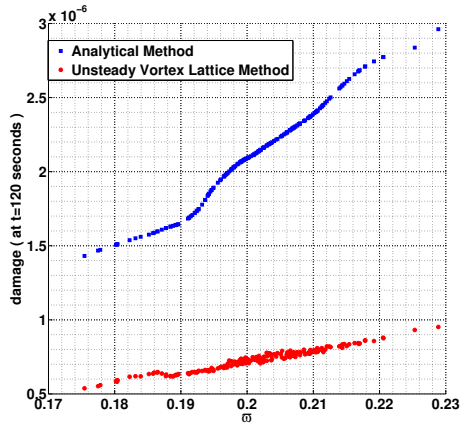
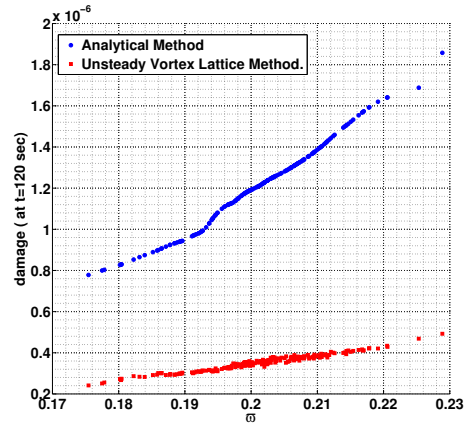


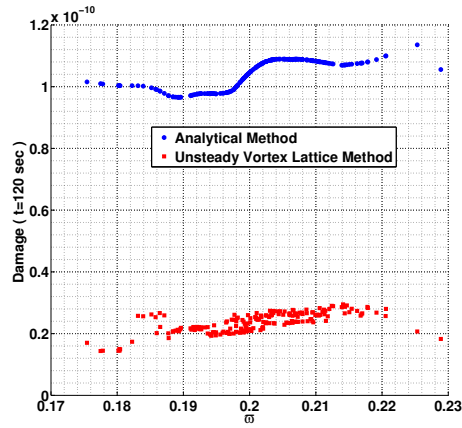
Figure 5: Signed vonMises stress calculation for a typical case.



(a) Signed vonMises

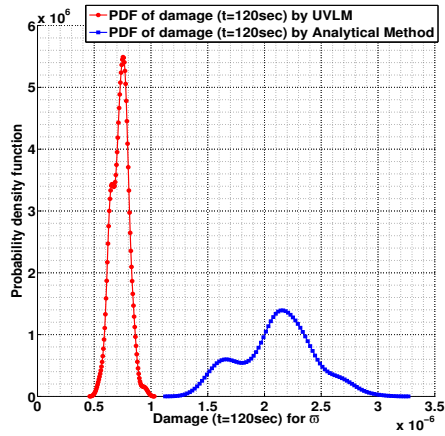


(b) Torsion

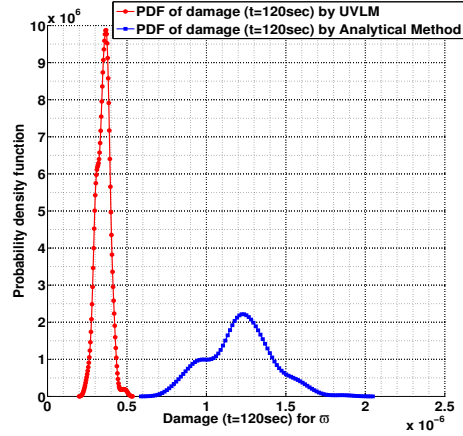


(c) Bending

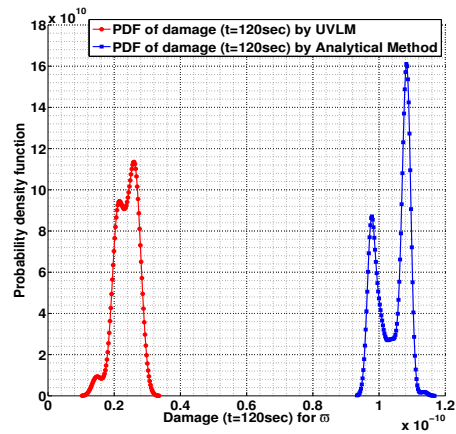
Figure 6: Damage pattern for random  $\bar{\omega}$  as predicted with (a) signed von-Mises, (b) torsion only, (c) bending only.



(a) Signed vonMises



(b) Torsion



(c) Bending

Figure 7: Damage PDF for random  $\bar{\omega}$  with (a) signed vonMises, (b) torsion only, (c) bending only and two models for environmental loads.

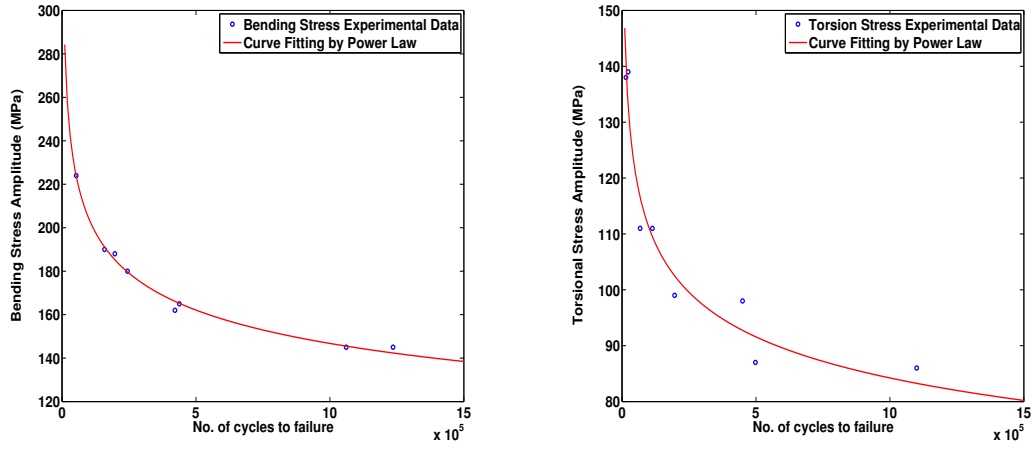


Figure 8: S-N data fit for bending and torsion stresses.

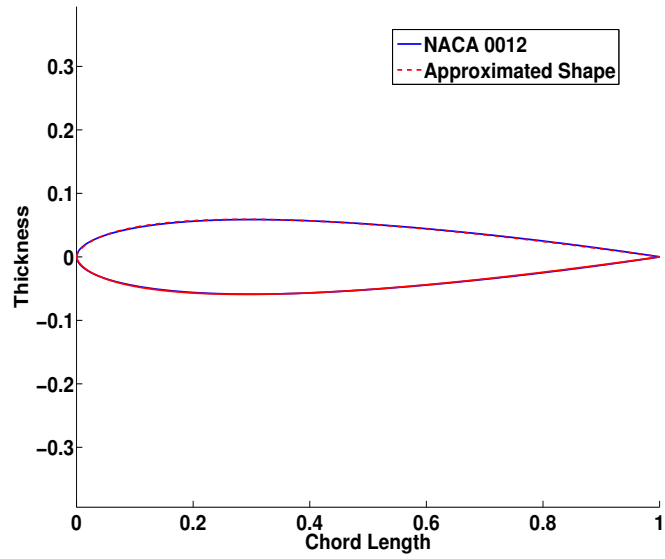


Figure 9: Comparison of actual NACA 0012 profile and its approximate fitted shape.

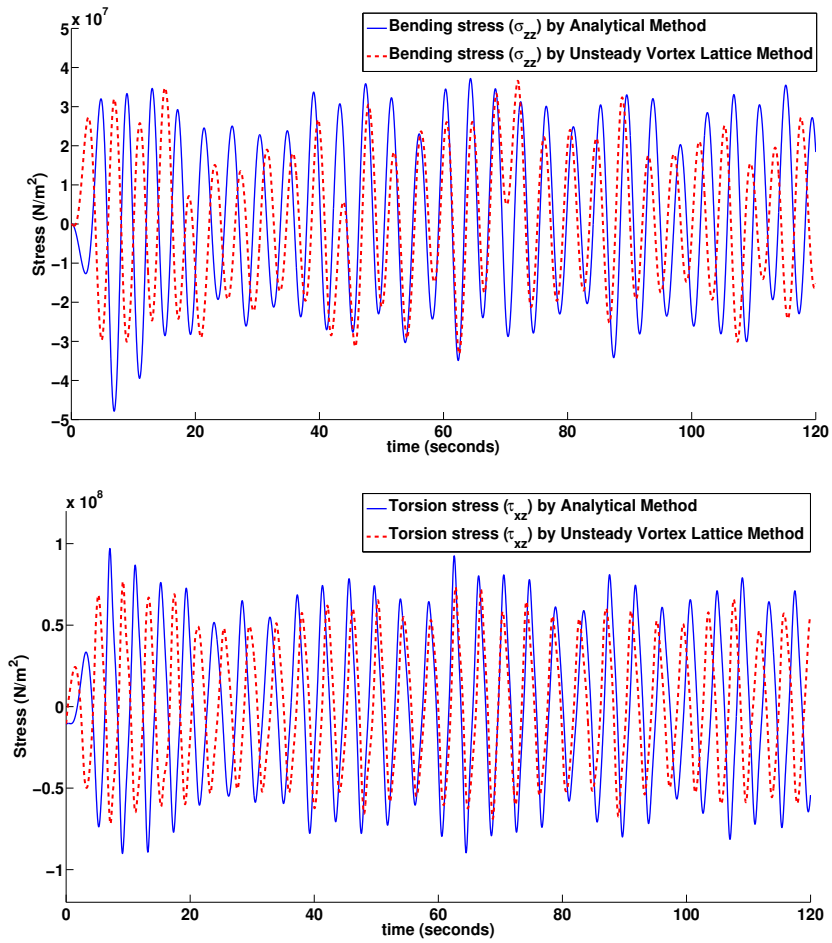


Figure 10: Typical stress time histories.